(Received 11 September 2024, Accepted 9 October 2024, Scheduled 14 October 2024)

Combining of Phase Cancellation and Absorption for Broadband High RCS Reduction Metasurface Design

Honggang Hao, Yi Shen*, Wen Huang, Siyao Li, and Zonggui Li

School of Optoelectronic Engineering, Chongqing University of Posts and Telecommunications, Chongqing, China

ABSTRACT: To enhance the reduction of radar cross section (RCS) and improve stealth performance, a phase cancellation and absorbing metasurface (PCAM) is designed in this paper. The PCAM is composed of a chessboard layout of circular units and square units, and it not only converts absorbed incident electromagnetic waves into heat to reduce the intensity of reflected electromagnetic waves but also simultaneously controls the phase of the reflected electromagnetic waves, achieving phase cancellation. This enables the metasurface to be exhibited with ultralow backscatter. After simulation verification, the metasurface can achieve RCS reduction of over 15 dB in the 4.3–11 GHz range for vertical incidence, with a fractional bandwidth of approximately 87.6% and over 15 dB in the 5.4–11.2 GHz range for a 30° oblique incidence, demonstrating good stability for oblique angles. The metasurface has increased the reduction level from over 10 dB to over 15 dB, significantly enhancing the RCS reduction. Additionally, in the co-planar state with a central curvature of 90°, it can also achieve RCS reduction of over 10 dB in the 3.2–9.9 GHz range, showing significant potential for practical applications.

1. INTRODUCTION

Metamaterials, also known as new artificial electromagnetic materials, are artificial composite materials composed of sub-wavelength unit structures, exhibiting characteristics of negative permittivity and negative permeability. Metasurfaces are a two-dimensional arrangement of artificial electromagnetic materials, possessing the unique ability to manipulate electromagnetic waves. Due to their distinctive capability to control electromagnetic waves [1, 2], metasurfaces hold significant potential in various applications, such as metasurfaces absorbers [3–5], polarization converters [6–8], and stealth cloaks [9, 10]. In recent years, metasurfaces as two-dimensional planar structures have become a focal point of research in RCS applications due to their lightweight nature, low profile, and ease of integration with device surfaces [11–17].

There are three main categories of methods using metasurfaces to achieve RCS reduction. The first method involves absorbing the energy of electromagnetic waves and converting it into heat to reduce the intensity of reflected waves [18, 19]. The second method involves controlling the backscattering of electromagnetic waves to deflect the primary energy of reflected electromagnetic waves away from the detection direction [20, 21]. The third method combines the first two mechanisms, absorbing waves while controlling backscattering [22]. Ji et al. utilized a two-layer structure. The first layer consisted of geometric phase units capable of scattering electromagnetic waves in the lower frequency range. The second layer was a resistive Frequency Selective Surface (FSS) enabling wave absorption in the higher frequency range, achieving a 10 dB RCS reduction in the 13–31.5 GHz range [23]. The two-layer structure improved performance, but it often increased complexity. Li et al. proposed a single-layer structure where a lumped resistor was inserted into the FSS. By adjusting the resistor values and the dimensions of the metallic structure, it achieved coherent absorption working together, resulting in over 15 dB RCS reduction in the 4.1–12.0 GHz band [24]. However, the designed metasurface only operated stably for x-polarized incidence. Moreover, in practical applications, metasurfaces often encounter significant influence in RCS reduction and bandwidth when being bent at large angles. Therefore, solving this problem is crucial [25, 26].

In this paper, we propose a single-layer PCAM structure composed of two types of FSS units with inserted lumped resistors. Due to its symmetrical design, it can operate stably under incoming waves of different polarizations. By combining absorption and phase cancellation mechanisms, this PCAM achieves over 15 dB RCS reduction in the 4.3–11 GHz range, significantly reducing backscattered energy. It also demonstrates stability at a 30° oblique incidence angle and can operate in conformal scenarios, thereby expanding its range of applications. It is suitable for stealth applications in the C-band, X-band, and parts of the S-band.

2. THEORY OF PCAM

The schematic diagram of the metasurfaces phase cancellation is shown in Fig. 1(a) with a checkerboard array structure where adjacent units have a certain phase difference. When electromagnetic waves vertically impinge on the checkerboard array, the reflected waves are divided into four lobes deviating from the central direction, as depicted in Fig. 1(b).

* Corresponding author: Yi Shen (syhxz823@126.com).

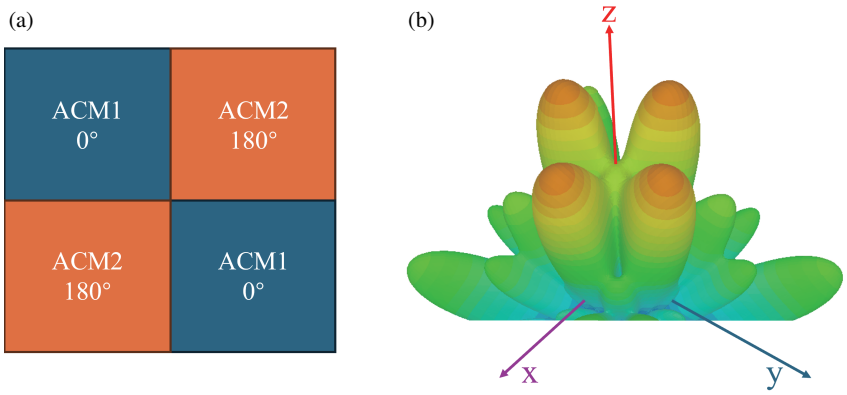

FIGURE 1. A checkerboard structure composed of two units with a 180° phase difference and their scattering pattern. (a) Checkerboard structure. (b) Scattering pattern.

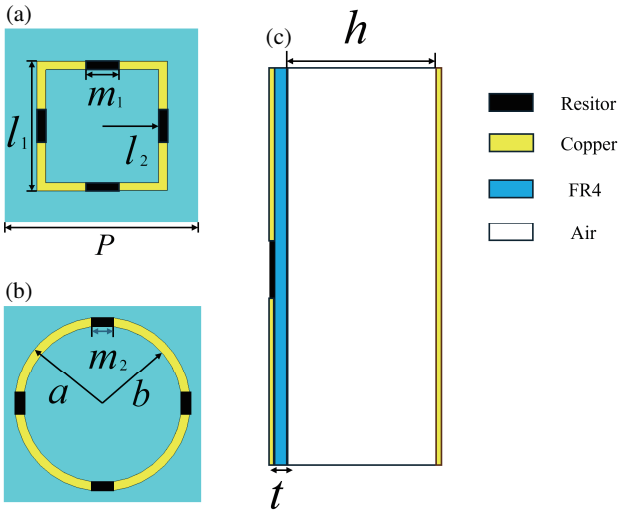

FIGURE 2. Unit structures. (a) Top view of unit 1. (b) Top view of unit 2. (c) Side view.

The reflected electromagnetic waves from the ACM1 unit and ACM2 unit can be expressed as:

$$\vec{E}_1 = \vec{A}_1 e^{j\varphi_2}, \quad \vec{E}_2 = \vec{A}_2 e^{j\varphi_2} \tag{1}$$

Here, A_1 and A_2 represent the amplitudes of the reflected waves, while φ_1 and φ_2 represent the phase of the reflected waves. Compared to a metallic plate of dimensions, the RCS reduction can be expressed as:

$$RCS_{redution} = 10\log\left(\frac{\left|\vec{A}_1 e^{j\varphi_1} + \vec{A}_2 e^{j\varphi_2}\right|}{\left|\vec{E}_r^{\text{Metal}}\right|}\right)^2 \tag{2}$$

where $\vec{E}_r^{\text{Metal}}$ represents the reflected electric field of the metal plate. From formula (2), it can be seen that the reduction in RCS not only is related to the phase of the unit, but also has an important connection with its reflection amplitude. When $A_1 = A_2 = 1$, to achieve an RCS reduction effect of more than 10 dB, the phase difference between the two units should be within the range of $180° \pm 37°$. If resistive elements are added to the unit or if resistive films are used instead of surface metal structures to give it absorbing characteristics, reducing the amplitude of the reflected wave, the RCS reduction effect will be further enhanced.

3. DESIGN OF METASURFACE UNIT

The structures of unit 1 and unit 2 are shown in Fig. 2(a) and Fig. 2(b). Due to the good angular and polarization stability of the circular and square ring FSS structures, along with a high operating bandwidth, the unit structures consist of metal square rings and metal circular rings with inserted lumped resistors. These structures are loaded on an FR4 ($\varepsilon = 4.3$) substrate with a thickness of $t = 0.4$ mm. Unit 1 and unit 2 have the same unit period $P = 18$ mm. Unit 1 features an open square ring structure with $l_1 = 12$ mm, $l_2 = 5.2$ mm, and an opening width of $m_1 = 3$ mm. Unit 2 is designed with an open circular ring structure with $a = 8$ mm, $b = 7.2$ mm, and an opening width of $m_2 = 2$ mm. Air isolation is used between the substrate and metal ground plane, with a thickness of $h = 9$ mm. The

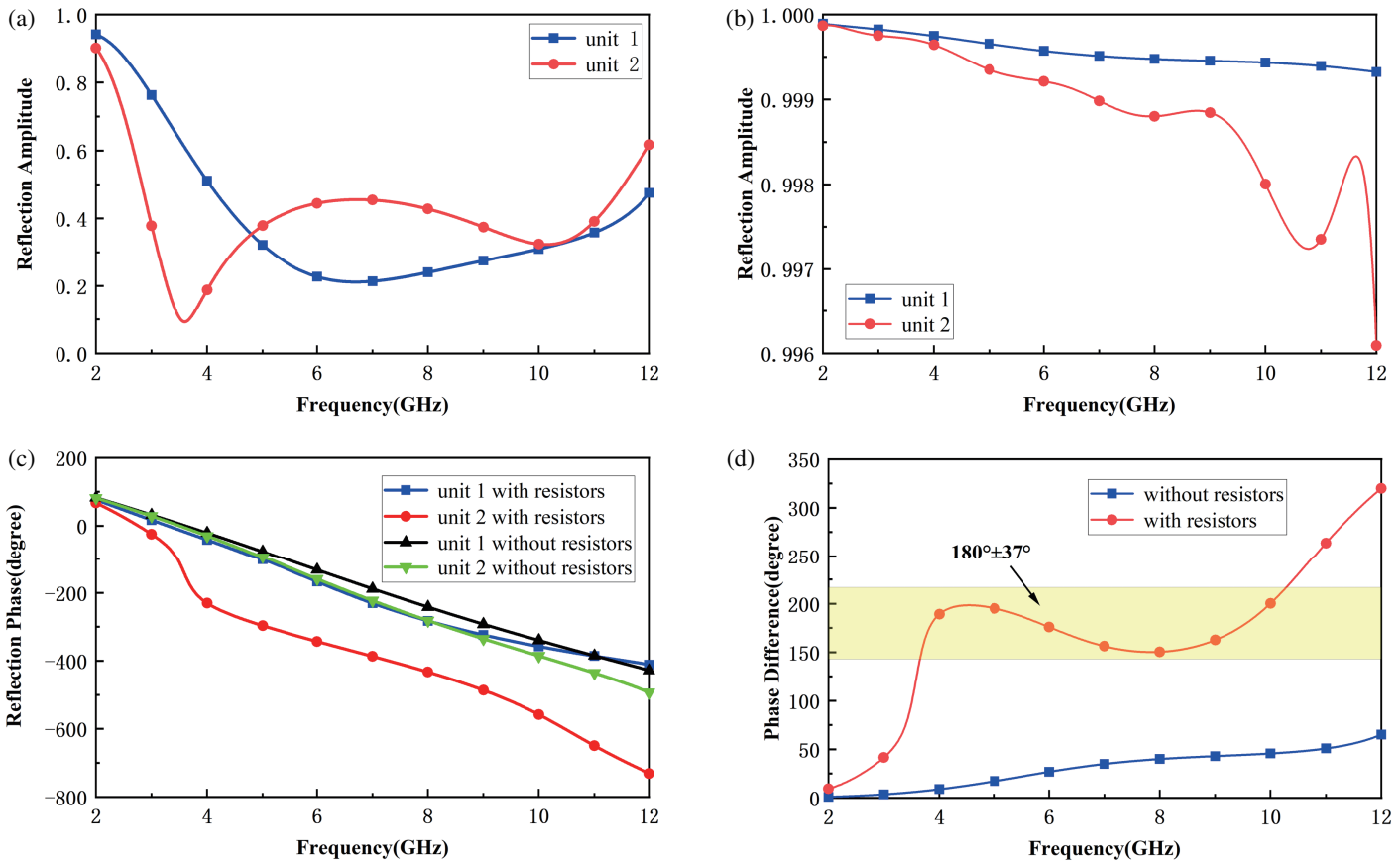

FIGURE 3. Reflection characteristics of the two units with or without resistors. (a) Reflection amplitude with resistors. (b) Reflection amplitude without resistors. (c) Reflection phase. (d) The phase difference between unit 1 and unit 2.

lumped resistor values for unit 1 and unit 2 are $R_1 = 350\,\Omega$ and $R_2 = 150\,\Omega$, respectively.

The reflection characteristics of units with and without resistors are shown in Fig. 3. The simulations in this paper are conducted using the commercial software CST Microwave Studio, with incident electromagnetic waves all being x-polarized. The reflection amplitude of the units with and without resistors are shown in Fig. 3(a) and Fig. 3(b), respectively. It can be observed that in the absence of resistors, the incident wave energy is almost entirely reflected, while with the insertion of resistors, a significant portion of the incident wave energy is absorbed by the resistors, converting into Ohmic losses. The phases of unit 1 and unit 2 are depicted in Fig. 3(c), and the phase difference is shown in Fig. 3(d). The phase difference of resistive unit 1 and unit 2 falls within $180° \pm 37°$ in the range of 3.6–10.3 GHz. The insertion of resistors not only enables the units to exhibit absorbing properties but also plays a crucial role in phase modulation, allowing the phase difference to approach 180° over a wider frequency band. By altering the physical dimensions of unit 1 and unit 2 as well as the resistance values of lumped resistors, favorable phase differences can be achieved while maintaining absorption performance during unit design. The metasurfaces that combine absorption and phase cancellation can further reduce the intensity of backscattered electromagnetic waves, thereby achieving better RCS reduction effects.

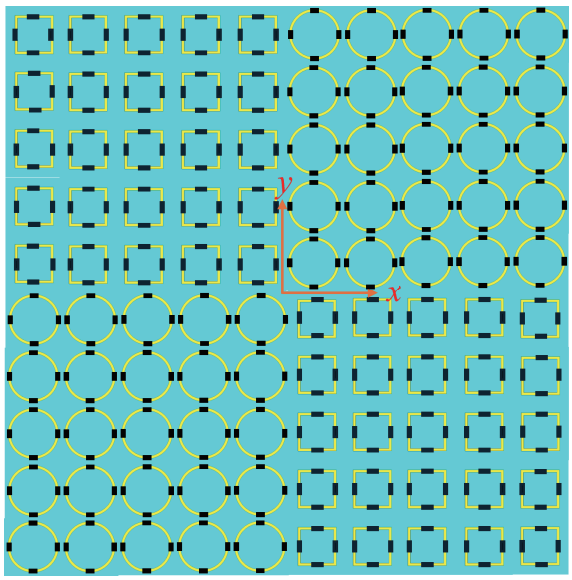

FIGURE 4. PCAM checkerboard array structure.

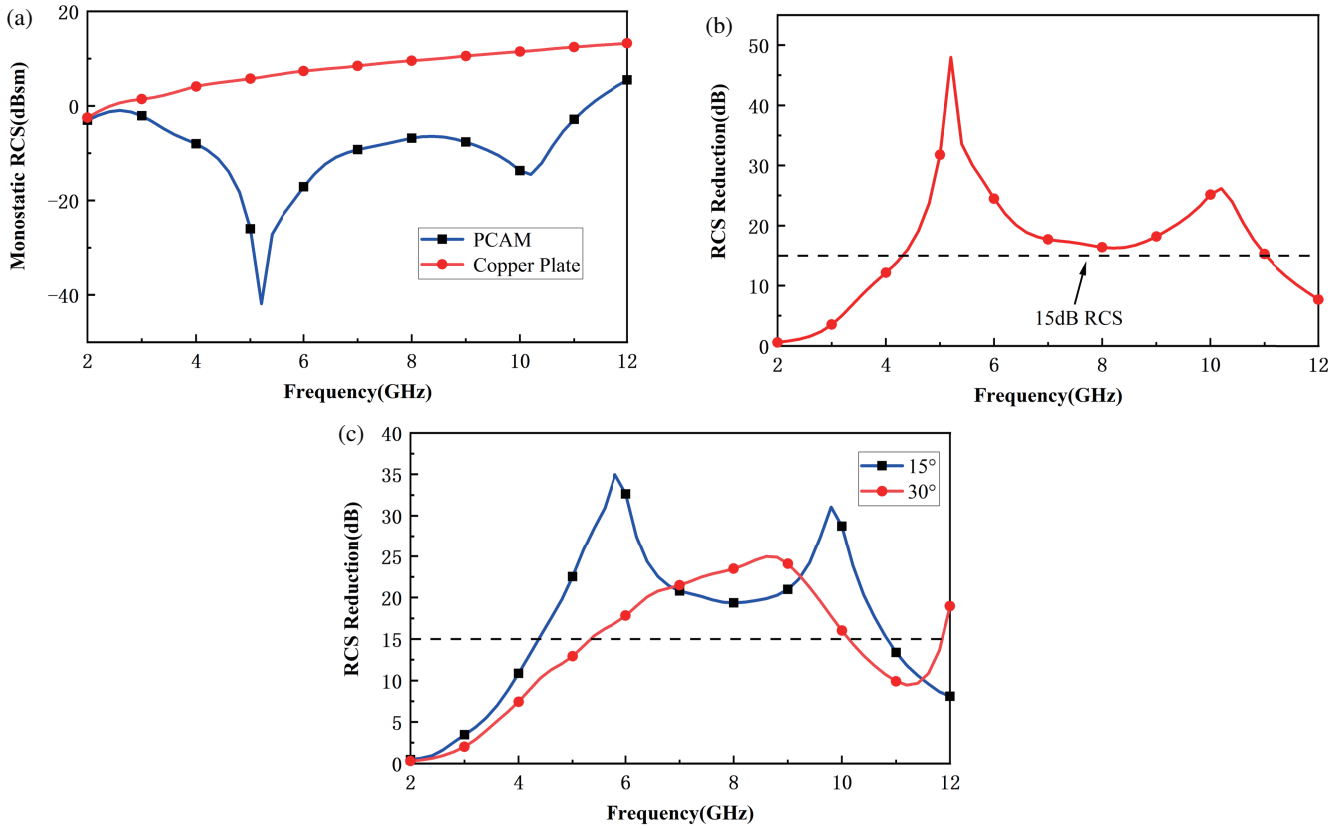

FIGURE 5. (a) Monostatic RCS of PCAM and metal plate. (b) Monostatic RCS reduction of PCAM. (c) RCS reduction in the mirror direction at 15° and 30° incident angles.

TABLE 1. Comparison of our paper and related designs.

Ref.	15 dB RCS Reduction FBW (%, GHz) Flat surface	Max angle	10 dB RCS Reduction FBW (%, GHz) Curved surface	Mechanism
8	Only point	No	No	Phase cancellation
13	77% (8.8–22)	20°	$\alpha = 90°$, 70% (9–16.7)	Phase cancellation
21	41% (18.4–27.9)	10°	No	Phase cancellation
22	Only point	45°	$\alpha = 60°$, 20% (19.4–23.6)	Hybird
23	16% (20.8–24.4)	20°	No	Hybird
This work	87.6% (4.3–11)	30°	$\alpha = 90°$, 102% (3.2–9.9)	Hybird

Ref: Reference, FBW: Fractional Bandwidth, α: Central curvature angle.

4. DESIGN OF PCAM AND SIMULATION

Building upon the unit design in the previous section, units 1 and 2 are arranged in a checkerboard pattern as shown in Fig. 1(a). Unit 1 and unit 2 are arranged in a 5×5 array to form a 10×10 checkerboard array, as shown in Fig. 4. The overall dimensions of the entire PCAM are 180 mm $\times$ 180 mm.

A metal plate of the same size is used as a control to compare the monostatic RCS in full-wave simulations for vertical incidence. The results are shown in Fig. 5(a). By subtracting the monostatic RCS of the metal plate from that of the PCAM, the monostatic RCS reduction curve of the PCAM in the range of 2–12 GHz is obtained, as shown in Fig. 5(b). It can be observed that a reduction of over 15 dB in RCS is achieved in the range of 4.3–11 GHz, with a fractional bandwidth of approximately 87.6%. Particularly, within the ranges of 4.7–6.4 GHz and 9.4–10.6 GHz, the RCS reduction exceeds 20 dB. For bistatic radar detection, non-specular scattered electromagnetic waves can be detected. However, it is well known that when the incident

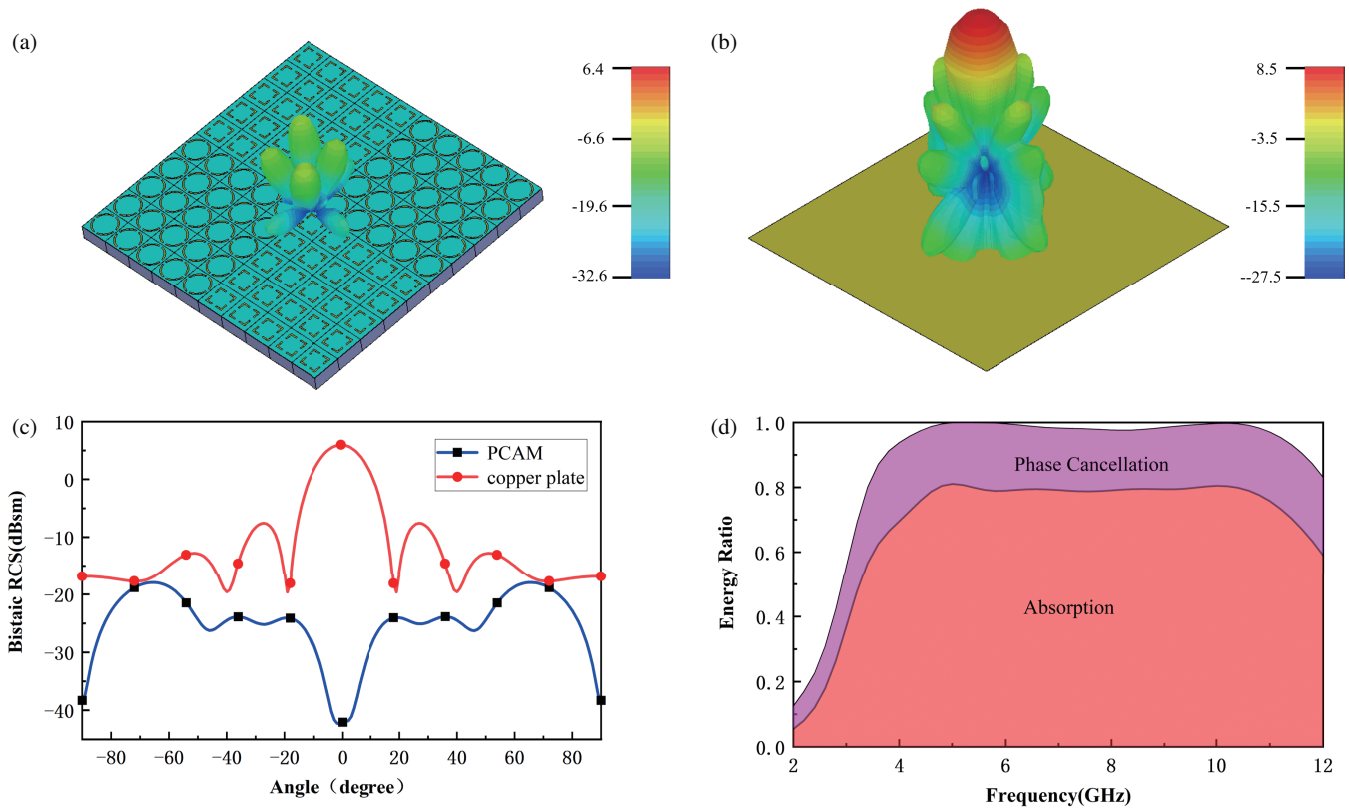

FIGURE 6. (a) 3D far-field pattern of PCAM (with resistors hidden). (b) 3D far-field pattern of metal plate. (c) Bistatic RCS of PCAM and metal plate. (d) Ratio of the phase cancellation and absorption of the PCAM under vertical incidence.

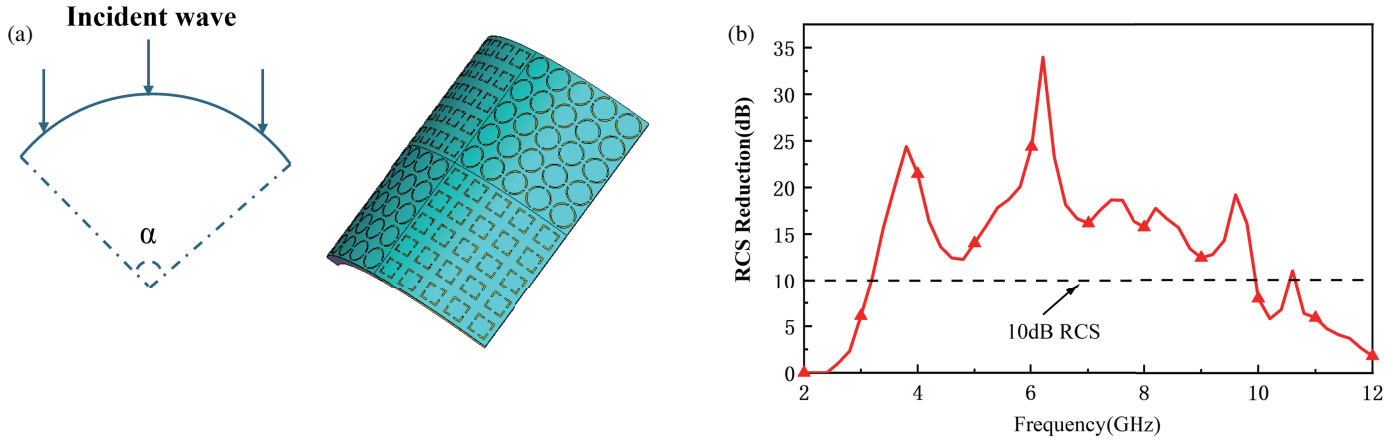

FIGURE 7. (a) PCAM structure with a central curvature angle $\alpha = 90°$ (with resistors hidden). (b) RCS reduction of curved PCAM.

wave is inclined to the metal surface, the scattered field is the strongest in the mirror reflection direction. In this case, stealth design mainly focuses on reducing the mirror RCS because non-specular scattering is much smaller than mirror scattering. Therefore, we further simulated the RCS reduction characteristics in the mirror direction at 15° and 30° incident angles. As shown in Fig. 5(c), a reduction of over 15 dB in RCS is still achieved in the 5.4–11.2 GHz range at a 30° incidence angle, with a reduction of 20 dB in RCS within the 6.4–9.5 GHz range, demonstrating good stability under oblique incidence.

Figure 6(a) presents the far-field simulation results of PCAM at 5.2 GHz under vertical incidence, contrasting with the metal plate as shown in Fig. 6(b). It can be observed that the designed metasurface not only possesses absorbing characteristics but also scatters the reflected energy in all directions, nearly eliminating the backscattered lobes. Fig. 6(c) shows the bistatic RCS of PCAM and the metal plate at phi = 90°, and the RCS is reduced in various directions. Fig. 6(d) depicts the ratio of absorption and phase cancellation in the vertically reduced en-

ergy, and it can be seen that both absorption and phase cancellation play important roles in RCS reduction.

In practical applications, many surfaces are curved, such as aircraft, radar domes, and ships. Metasurfaces need to conform to the surfaces of objects, so they also need to adapt to curved shapes. Therefore, the planar PCAM is introduced onto a cylindrical surface with a central angle $\alpha = 90°$ as shown in Fig. 7(a).

Under vertical incidence, a comparison with a metal curved surface with the same curvature angle yields RCS reduction curves as shown in Fig. 7(b). It can be observed that with the curved PCAM loaded, a reduction of over 10 dB in RCS is achieved in the range of 3.2–9.9 GHz, with a relative bandwidth of approximately 102.2%. Although the RCS reduction effect is slightly lower than the planar PCAM, it still meets expectations.

Table 1 lists the comparison between our research and other relevant studies on conventional phase cancellation metasurfaces [8, 13, 21] and hybrid mechanism metasurfaces [22, 23]. The designed metasurface shows significant advantages in terms of reduction amount and operating bandwidth.

5. CONCLUSION

In this paper, a phase cancellation and absorbing metasurface is proposed, which enhances the reduction effect of RCS by absorbing incident electromagnetic waves and further controlling backscattered electromagnetic waves through phase cancellation. Through simulation verification, this PCAM achieves a reduction of over 15 dB in RCS in the 4.3–11 GHz range, with a fractional bandwidth of approximately 87.6%. Moreover, at a 30° oblique incidence, it still maintains a reduction of over 15 dB in RCS in the 5.4–11.2 GHz range, demonstrating good stability under oblique incidence. Additionally, when the metasurface is applied to a cylindrical surface with a central curvature angle of 90°, it achieves a reduction of over 10 dB in RCS in the 3.2–9.9 GHz range, with a fractional bandwidth of approximately 102.2%, expanding its application scenarios. The proposed metasurface structure is simple and reliable in performance. It can be applied to stealth applications in the C, X, and some S bands.

ACKNOWLEDGEMENT

This work was supported by Chongqing Natural Science Foundation General Program (CSTB2022NSCQ-MSX0960) and Scientific and Technological Research Program of Chongqing Municipal Education Commission (KJQN202300611).

REFERENCES

[1] Genevet, P., F. Capasso, F. Aieta, M. Khorasaninejad, and R. Devlin, "Recent advances in planar optics: From plasmonic to dielectric metasurfaces," *Optica*, Vol. 4, No. 1, 139–152, 2017.

[2] Zhou, Y., X. Cao, J. Gao, H. Yang, and S. Li, "Reconfigurable metasurface for multiple functions: Magnitude, polarization and phase modulation," *Optics Express*, Vol. 26, No. 22, 29 451–29 459, 2018.

[3] Cao, H., M. Shan, T. Chen, J. Lei, L. Yang, and X. Tan, "Triple-band polarization-independent ultrathin metamaterial absorber," *Progress In Electromagnetics Research M*, Vol. 77, 93–102, 2019.

[4] Ranjan, P., A. Choubey, S. K. Mahto, and R. Sinha, "An ultrathin five-band polarization insensitive metamaterial absorber having hexagonal array of 2D-bravais-lattice," *Progress In Electromagnetics Research C*, Vol. 87, 13–23, 2018.

[5] Xu, G., J. Huang, Z. Ju, Z. Wei, J. Li, and Q. Zhao, "A novel six-band polarization-insensitive metamaterial absorber with four multiple-mode resonators," *Progress In Electromagnetics Research C*, Vol. 77, 133–144, 2017.

[6] Lei, Z. and T. Yang, "Converting state of polarization with a miniaturized metasurface device," *IEEE Photonics Technology Letters*, Vol. 29, No. 7, 615–618, 2017.

[7] Cai, T., G.-M. Wang, X.-L. Fu, J.-G. Liang, and Y.-Q. Zhuang, "High-efficiency metasurface with polarization-dependent transmission and reflection properties for both reflectarray and transmitarray," *IEEE Transactions on Antennas and Propagation*, Vol. 66, No. 6, 3219–3224, 2018.

[8] Murugesan, A., D. Natarajan, and K. T. Selvan, "Low-cost, wideband checkerboard metasurfaces for monostatic RCS reduction," *IEEE Antennas and Wireless Propagation Letters*, Vol. 20, No. 4, 493–497, 2021.

[9] Yang, J., C. Huang, X. Wu, B. Sun, and X. Luo, "Dual-wavelength carpet cloak using ultrathin metasurface," *Advanced Optical Materials*, Vol. 6, No. 14, 1800073, 2018.

[10] Han, N., L. Huang, and Y. Wang, "Illusion and cloaking using dielectric conformal metasurfaces," *Optics Express*, Vol. 26, No. 24, 31 625–31 635, 2018.

[11] Zheng, Y., X. Cao, J. Gao, H. Yang, Y. Zhou, and S. Wang, "Shared aperture metasurface with ultra-wideband and wide-angle low-scattering performance," *Optical Materials Express*, Vol. 7, No. 8, 2706–2714, 2017.

[12] Liu, X., J. Gao, L. Xu, X. Cao, Y. Zhao, and S. Li, "A coding diffuse metasurface for RCS reduction," *IEEE Antennas and Wireless Propagation Letters*, Vol. 16, 724–727, 2016.

[13] Chatterjee, J., A. Mohan, and V. Dixit, "Ultrawideband RCS reduction of planar and conformal surfaces using ultrathin polarization conversion metasurface," *IEEE Access*, Vol. 10, 36 563–36 575, 2022.

[14] Al-Nuaimi, M. K. T., W. Hong, and Y. He, "Backscattered EM-wave manipulation using low cost 1-bit reflective surface at W-band," *Journal of Physics D: Applied Physics*, Vol. 51, No. 14, 145105, 2018.

[15] Feng, M., Y. Li, Q. Zheng, J. Zhang, Y. Han, J. Wang, H. Chen, S. Sai, H. Ma, and S. Qu, "Two-dimensional coding phase gradient metasurface for RCS reduction," *Journal of Physics D: Applied Physics*, Vol. 51, No. 37, 375103, 2018.

[16] Al-Nuaimi, M. K. T., W. Hong, and Y. He, "Design of diffusive modified chessboard metasurface," *IEEE Antennas and Wireless Propagation Letters*, Vol. 18, No. 8, 1621–1625, 2019.

[17] Hao, H., S. Du, and T. Zhang, "Small-size broadband coding metasurface for RCS reduction based on particle swarm optimization algorithm," *Progress In Electromagnetics Research M*, Vol. 81, 97–105, 2019.

[18] Li, M., S. Xiao, Y.-Y. Bai, and B.-Z. Wang, "An ultrathin and broadband radar absorber using resistive FSS," *IEEE Antennas and Wireless Propagation Letters*, Vol. 11, 748–751, 2012.

[19] He, Y., W. Feng, S. Guo, J. Wei, Y. Zhang, Z. Huang, C. Li, L. Miao, and J. Jiang, "Design of a dual-band electromagnetic absorber with frequency selective surfaces," *IEEE Antennas and Wireless Propagation Letters*, Vol. 19, No. 5, 841–845, 2020.

[20] Yu, H., J. Su, Q. Guo, and Z. Li, "Dual wideband, polarization, angle-insensitive diffusion electromagnetic surfaces for radar cross section reduction," *Journal of Physics D: Applied Physics*, Vol. 54, No. 20, 205102, 2021.

[21] Liu, J., J.-Y. Li, and Z. N. Chen, "Broadband polarization conversion metasurface for antenna RCS reduction," *IEEE Transactions on Antennas and Propagation*, Vol. 70, No. 5, 3834–3839, 2022.

[22] Chang, Q., J. Ji, and Y. Ma, "Transparent and flexible chessboard metasurface based on optimized multielement phase cancellation for wideband RCS reduction," *IEEE Access*, Vol. 12, 27 887–27 894, 2024.

[23] Ji, C., C. Huang, X. Zhang, J. Yang, J. Song, and X. Luo, "Broadband low-scattering metasurface using a combination of phase cancellation and absorption mechanisms," *Optics Express*, Vol. 27, No. 16, 23 368–23 377, 2019.

[24] Li, C., Z. Xu, L. Lin, S. Guo, Y. He, L. Miao, and J. Jiang, "Ultralow scattering and broadband metasurface using phase adjustable FSS elements embedded with lumped resistors," *IEEE Antennas and Wireless Propagation Letters*, Vol. 20, No. 5, 793–797, 2021.

[25] Khan, H. A., A. Majeed, H. Zahra, F. G. Kakepoto, S. M. Abbas, and M. Alathbah, "Transparent conformal metasurface absorber for ultrawideband radar cross section reduction," *Journal of Physics D: Applied Physics*, Vol. 57, No. 13, 135105, 2024.

[26] Lai, S., Y. Wu, J. Wang, W. Wu, and W. Gu, "Optical-transparent flexible broadband absorbers based on the ITO-PET-ITO structure," *Optical Materials Express*, Vol. 8, No. 6, 1585–1592, 2018.